Received: 30 April 2019 | Revised: 26 June 2019 | Accepted: 29 July 2019

DOI: 10.1002/jbio.201900166

FULL ARTICLE

JOURNAL OF BIOPHOTONICS

Designable nanoplasmonic biomarkers for direct microscopy cytopathology diagnostics

Lu Wang[1] | **Cecile Darviot**[1] | **Jennyfer Zapata-Farfan**[1] | **Sergiy Patskovsky**[1] | **Dominique Trudel**[2] | **Michel Meunier**[1*]

[1]Laser Processing and Plasmonics Laboratory, Department of Engineering Physics, Polytechnique Montréal, Montréal, Québec, Canada

[2]Research Center of the Centre Hospitalier de l'Université de Montréal (CHUM), Montreal, Québec, Canada

*Correspondence
Michel Meunier, Laser Processing and Plasmonics Laboratory, Department of Engineering Physics, Polytechnique Montréal, C.P. 6079, Succ. Centre-ville, Montréal, Québec H3C 3A7, Canada.
Email: michel.meunier@polymtl.ca

Funding information
CIHR; FRQNT; FRQS; NSERC

Abstract

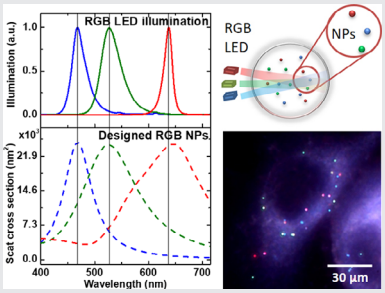

Direct microscopy interpretation of fine-needle biopsy cytological samples is routinely used by practicing cytopathologists. Adding possibility to identify selective and multiplexed biomarkers on the same samples and with the same microscopy technique can greatly improve diagnostic accuracy. In this article, we propose to use biomarkers based on designable plasmonic nanoparticles (NPs) with unique optical properties and excellent chemical stability that can satisfy the above-mentioned requirements. By finely controlling the size and composition of gold-silver alloy NPs and gold nanorods, the NPs plasmonic resonance properties, such as scattering efficiency and resonance peak spectral position, are adjusted in order to provide reliable identification and chromatic differentiation by conventional direct microscopy. Efficient darkfield NPs imaging is performed by using a novel circular side illumination adaptor that can be easily integrated into any microscopy setup while preserving standard cytopathology visualization method. The efficiency of the proposed technology for fast visual detection and differentiation of three spectrally distinct NP-markers is demonstrated in different working media, thus confirming the potential application in conventional cytology preparations. It is worth emphasizing that the presented technology does not interfere with standard visualization with immunohistochemical staining, but should rather be considered as a second imaging modality to confirm the diagnostics.

KEYWORDS
Au/Ag alloy, biomarker, cytology diagnostics, nanoparticles, plasmonic

1 | INTRODUCTION

Recent decades have seen the bloom of development of plasmonic nanoparticles (NPs), being rapidly applied in various fields, such as catalysis [1–3], optics [4], and biomedicine [5, 6]. Due to their tremendous scattering efficiency, structural designability, optical tunability [7], and surface functionalization ability [8–11], colloidal plasmonic NPs and regular nanoplasmonic structures have brought new opportunities to a number of areas and opened doors for substantial challenges [12]. Through designing the size, shape, and composition of plasmonic NPs, various types of plasmonic NPs

have been engineered with specific plasmonic properties addressing different applications [5, 13–15].

Under illumination and detection, the noble metal NPs strongly scatter light and have 10^5 to 10^6 times higher scattering cross section than conventionally used fluorophores when used in bioimaging [8, 16]. Additionally, they are not subject to blinking and bleaching effects, offering an extraordinary photostability for imaging and biosensing. Optical encoding strategies of plasmonic NPs are based on dark field microscopy (DFM) methods that, in combination with hyperspectral scanning sources or cameras, allow efficient spectral differentiation, precise spatial localization, and multiplexed quantification of NP-based biological labels [17–19].

Nowadays, there is a need for cost-effective, sensitive, and specific diagnostic methodology to overcome the limitations associated with conventional cyto- and histo-pathology based methods. Due to the high scattering efficiency and photostability of plasmonic NPs, there exist many successful applications in bioimaging [20, 21]. We think that a methodology based on a cytology protocol, where cell immunolabeling is performed by means of plasmonic NPs can drastically improve diagnostic reliability. However, to promote user adoption of this new method in cytopathology laboratories, the NPs imaging hardware should be simple and compatible with equipment currently used in laboratories. Likewise, the sample preparation and imaging procedure should not involve additional steps or risks of sample contamination compared with the existing procedures. Moreover, the practicing pathologists want to observe and differentiate multiple NPs labels directly at the eyepiece of the microscope, as well as comparing and combining the images with the conventional bright field observation mode. With the aim of realizing this idea, we recently introduced a darkfield lateral illumination approach and compact device for multispectral NPs detection without the cumbersome equipment required for conventional DFM visualization [22]. We paid particular attention to the fact that the new modality should not interfere with the standard method. The proposed method was based on the chromatic differences of three NPs: Au, Ag and Au nanorods that with consecutive illumination by means of blue, red and green light from Red-Green-Blue (RGB) Light-emitting diodes (LED), allowed reliable plasmonic labels identification. By simply switching between lateral illumination and traditional brightfield illumination, the pathologists may opt for immunohistochemistry or immunoplasmonic imaging at their convenience. However, fast visual simultaneous NPs identification was still problematic due to the low coupling between the optimal spectral signature of the NPs and the RGB LED source.

Digital pathology appears as a promising trend for pathology; however, there are still many problems before it becomes widespread. The most concerned problems involve the variation of sample preparation and parameters in digitalization process, which requires general algorithm to compensate their influences. Moreover, digitalization is a time-consuming task, especially for obtaining more details and accurate information, which is an inevitable part of database building [23]. Therefore, most pathologists rely much more on their experience with familiar methods of sample preparation as well as the visualization. Our technique responds to the urgent needs of direct visualization and providing at the same time a compatible way of low-cost digitalization.

In this article, we first theoretically predicted and experimentally synthesized two gold-silver (Au/Ag) alloy NPs with designed composition and sizes that together with Au nanorods NPs can be used as three spectrally distinct biomarkers optimized for direct microscopy cytopathology analysis. We then investigated the influence of three different surrounding media on the NPs parameters: PBS buffer solution for live cells detection, mounting medium solution for cytopathology tests mimicking clinical situations, and oil for the best NPs imaging contrast. We have also developed a circular side-illumination (CSI) adaptor as an improved darkfield microscopy methodology for the rapid visual multispectral identification of individual plasmonic NPs in live or fixed cell samples. We believe that the proposed technology can facilitate and accelerate the adoption of a new type of reliable and stable biomarkers for ex-vivo cytopathology analysis and diagnostics, where possible toxicity of NPs cannot drastically influence obtained results.

2 | MATERIALS AND METHODS

2.1 | Materials

All chemical reagents were used as received, without further purification. Gold (III) chloride trihydrate ($HAuCl_4 \cdot 3H_2O$, ≥99.9%) was purchased from Sigma-Aldrich, silver nitrate ($AgNO_3$, 99.995%) and trisodium citrate dihydrate ($Na_3C_6H_5O_7 \bullet 2H_2O$, 99.0%) were obtained from Alfa Aesar. Before synthesis experiments, all glassware was cleaned with aqua regia and rinsed thoroughly with deionized water. All water used in this work is provided by Millipore Direct Q-UV3 water purification system, as ultrapure water with 18 MΩ resistivity. Nanorods (A12-40-600 and A12-40-650) were purchased from Nanopartz. Circular glass slides and coverslip (25 mm in diameter) were used for NPs and cell samples preparation. VECTASHIELD Vibrance Antifade Mounting Medium was purchased from Biolynenx Inc., which was chosen as the representative mounting medium for fixed-cell samples and is hereinafter referred as mounting medium. MDA-MB-231 cell line from ATCC was cultured for cell samples. “Culture-Inserts 2 Well for self-insertion” from

Ibidi were used for culturing the cells on slides for sample preparation.

2.2 | Synthesis of Au/Ag NPs

Spherical Au/Ag NPs of controlled size and composition were synthesized by optimizing the previously reported method (seeded growth combined with coreduction method) [24]. Based on that, multiple injection in each growth stage were performed in a controlled manner in order to keep a low concentration of free ions, thus avoiding a secondary nucleation. Moreover, temperature was controlled in a dynamic way according to the ingredient injection status to regulate the rate of chemical reduction and NPs growth for precise shape control.

First, Gold (Au) seeds are synthesized through Turkevich method, as mentioned in existing work [24, 25]. In the protocol, 300 μL 30 mM $HAuCl_4$ water solution and 200 μL 170 mM $Na_3C_6H_5O_7$ (NaCit) water solution were added into 30 mL of boiling water. Keeping boiling for 15 to 30 minutes, Au seeds were synthesized with 15 ± 1 nm in diameter. The volume of seeds solution was adjusted to 30 mL by adding water in order to achieve an atomic concentration of 300 μM.

Then, 2 to 3 growth stages were performed to reach the final size. Typically, in the first growth stage, 3 mL Au seeds achieved in initial seeds synthesis were dispersed into 57 mL 90°C water in three-necked flask with heating bath and refluxing. Reducing agent 540 μL 170 mM NaCit and metal precursors 270 μL $HAuCl_4$ (30 mM) and $AgNO_3$ (30 mM) solution (in corresponding ratio of Au/Ag for the designed composition) was added in ten successive injections. After all injections, heating temperature was raised up to 100°C to keep boiling for 1 hour. Then alloy NPs, with 32 ± 2 nm diameter, were synthesized, which can be used as seeds for the next growth stage. NaCit was added before metal salts in order to adjust the pH to slow down the chemical reduction velocity, thus facilitating homogeneous growth of NPs [26–28]. For following growth stage(s), NPs synthesized in the last stage were used as seeds, and a similar process was performed to obtain the designed bioimaging labels.

In the growth stage, in order to avoid aggregation or undesired nucleation, total concentration of metal atoms should be limited to 150 μM, including Au and Ag in seeds and injected metal precursors [24]. Based on our experimental results, in each growth stage, the volume ratio of final NPs compared with the seeds should be limited to 10 to ensure that the required size distribution is less than 10%. With the first growth stage, we obtained NPs with 32 ± 2 nm diameter, which can be used as seeds in the second growth stage, resulting in NPs with diameter of 69 ± 4 nm. For even larger NPs, another growth stage will be necessary.

2.3 | Characterization of NPs

The spectrum of colloidal NPs in water was measured with an Epoch Microplate Spectrophotometer. The morphology and size of the NPs were characterized by transmission electron microscope (TEM, JEOL 2100), and Energy-dispersive X-ray spectroscopy (EDS) was also performed on the samples to define the composition of Au/Ag alloy NPs. The samples were prepared on a Cu grid with thin carbon film (Cu-400CN, Pacific grid tech) dipped into ethanol dispersions and air-dried for every synthesized sample (Au/Ag alloy NPs).

To prepare the sample of NPs within targeting media, 3 μL of aqueous NPs solution was dropped on a microscope slide and subsequently dried with compressed nitrogen. After this procedure, 40 μL of targeting medium were deposited on the slide to cover the NPs area. A 120 μm double-sided spacer tape was set on the slide in order to cover the sample. Scattering spectrum from single NPs was then acquired through backreflection with a 100× oil objective and Andor Shamrock SR-750 imaging spectrophotometer under the illumination of an halogen lamp [29]. An inverted Nikon microscope equipped with 60× air objective combined with side illumination adaptor was employed for NPs and cells samples visualization, and the commercial camera Nikon D7500 was used for taking digital photos.

2.4 | Cell sample preparation

MDA-MB-231 cells were used as cytology samples in this work. The cells were cultured on circular slides confined in self-insert well. When the confluence reached around 80%, three types of NPs mixed in the culture medium were added into the well. After 2 hours of incubation, free NPs were washed three times with PBS and fixed with methanol. After another washing with PBS, the well was removed and replaced by a double-sided spacer adding the proper medium: PBS, mounting medium or oil, to subsequently use a coverslip for sealing the sample.

2.5 | Side-illumination adaptor for dark field NPs microscopy

For this work, we designed a new microscopy adaptor where side illumination is adjusted to the circular 25 mm diameter 1 mm thick glass microscope slide with optically polished sides. The substrate is compatible with conventional 25 mm microscopy coverslips for sample preparation. As a light source, we used high-performance tricolor Cree CLS6B

LEDs with a wide viewing angle and high brightness. In the design, the narrow RGB LED array (LED size: 4.7 × 1.5 × 1.3 mm) was mounted in close optical contact with the border of the circular microscope slide, as shown schematically in Figure 1A. In order to provide the required precision by the scientific grade microscopes, the working prototype (Figure 1B) was fabricated (Vegaphoton Inc.) using aluminum CNC machining for a Nikon inverted microscope. Our tests confirmed theoretical estimation (Zemax optical software) in 3.6 times increased power in intensity and more homogeneous illumination for circular side illumination compared to the previously published rectangular configuration [22]. Another advantage of the circular illumination is the minimization of the influence of the spatial orientation of such plasmonic nanomarkers as Au nanorods on the scattering spectral dependences.

An important property of NPs darkfield microscopy with side illumination is its compatibility with most optical microscopes commonly used by researchers and pathologists. This approach and device can be implemented with a standard protocol for cytopathology sample preparation. The visualization method allows simple switching or even combination between conventional transmission mode microscopy and side illumination dark field mode, thus providing complete and more reliable sample analysis.

RGB LED have emission peaks at 638 nm, 526 nm and 468 nm corresponding to R, G and B illumination, respectively. To provide the flexibility in the intended direct visualization microscopy, the manual control of the intensity of the individual color LED is possible. This adaptor can also be used for the realization of an automatic digital NPs microscopy where LED color, intensity, and imaging CMOS color or monochromatic camera will be controlled by the corresponding external software.

3 | RESULTS AND DISCUSSION

3.1 | Design of optimized NPs for three mediums

The main goal of this project is to provide a scientist, and ultimately a practicing pathologist, a protocol and a useful tool for fast medical diagnostics based on direct visual observation of multiplexed plasmonic biomarkers. To make it possible, such plasmonic biological labels should respond to multiple criteria. First, optical labels must be clearly visible by using simplified darkfield microscopy. This requires high enough scattering efficiency, or scattering cross section, which depend on dimension and composition of NPs [16, 30, 31]. As stands out from the literature, NPs scattering efficiency comparable to the rather large 100 nm Au NPs (~37 300 nm^2) can fulfill such requirement [22, 32]. In addition, NPs are designed to target the receptors on the cell membrane. Their relatively large sizes can prevent endocytosis with living cells, which can significantly change the expression of proteins and lead to an inaccurate quantitative determination of surface receptors [33, 34]. Second, multiplexed NP markers have to be easily chromatically differentiated. Separated resonance peaks are required, which means large difference between peak positions and small overlap for the whole spectra. This requirement is setting a limitation on the number of simultaneously detected NPs, since the spectra of the resonance peak broaden with NP size as well as the distribution of NPs size and composition. Also, the size of NPs cannot be too large, in order to avoid obvious quadrupole peak, which determines our choice of 100 nm Au NPs as reference for the scattering cross section and spectral shape of plasmonic peak. Moreover, the quality control of NPs is important, to obtain narrow distribution of size and composition. Third, the NP scattering colors should stay in the visible range for simplified direct chromatic differentiation and, at the same time, be finely tuned to the emission spectra of the commercially available miniature RGB LED. Therefore, the exact matching of the NPs scattering peak position with emission peak of individual LED is a required optimization condition for NPs fabrication.

Depending on the application, research and diagnostic protocols can be performed with plasmonic biomarkers in different surrounding media that influence their plasmonic and spectral properties. For example, if the 3D spatial distribution of NPs is investigated, the highest possible contrast is provided by matching refractive indexes (RI) between the glass substrate and the oil medium, as they have very close RI. A PBS solution with RI of about 1.34 is often used in the case of live cell manipulation and labeling with NP markers. Finally, conventional cytopathology samples are

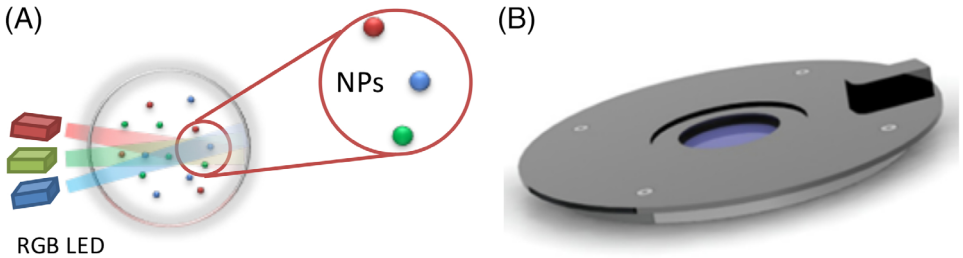

FIGURE 1 A, Principle of circular side illumination (CSI) microscopy with RGB LED side illumination and plasmonic NPs as biomarkers; B, experimental prototypes of CSI adaptor compatible for conventional optical microscopy

commonly prepared using mounting medium to fix and preserve cells on microscope slides. All these three media: PBS, cell mounting medium and oil are of particular interest to this project and, correspondingly, all of the above requirements for NP specifications as biomarkers need to be readjusted based on the application and used medium.

The spectral position of metallic NPs plasmonic peak can be tuned in a large spectral range depending only on the size for spherical NPs. However, adjusting the NP size is not sufficient to respond to all of the above-mentioned criteria and particularly to provide similar scattering efficiency from one marker type to another. In this article, we propose to use alloy Au/Ag NPs that, as was recently shown [24], can provide much more flexibility in fine spectral tuning by changing NP size and composition. Using Mie theory adapted to alloy NPs we have performed theoretical calculation and found the optimal alloy NP parameters to match blue (468 nm) and green (526 nm) LED illumination in different surrounding media. For future applications, if necessary, the thin biofilm of NP functionalization will be included in the optimization of the NP design and corresponding synthesis protocol.

However, alloy Au/Ag NPs tuning capabilities are limited in terms of wavelength range. For the requirements mentioned above, the highest wavelength we can reach is around 580 nm, which corresponds to pure gold NPs of about 100 nm. Therefore, for the case of red LED lighting (638 nm), we suggest using Au nanorods, where the scattering efficiency and spectral dependences can be adjusted in accordance with our requirements. Based on Mie theory and the dielectric function for Au/Ag alloy [35, 36], we have performed a theoretical calculation of the alloy NPs diameter and scattering cross section dependences on the Au/Ag composition for the fixed NPs resonance peak position that correspond to blue and green illumination in three working media. Figure 2 shows example of obtained results for alloy NPs in PBS medium. For the reliable NPs detection, we chose as the reference as scattering cross section of the 100 nm Au NPs (the red horizontal line on the figure). Aiming at having similar scattering cross sections, one can easily obtain the composition and diameter of optimal NPs, as shown in the figure. For example, the optimal size for the "green" NPs is 99 nm in diameter with Au/Ag composition 49/51. Furthermore, for the "blue" NPs calculation shows that the pure Ag NPs are preferable. However, our preliminary experimental results on the stability of fabricated alloy NPs (not presented here) have shown that pure silver NPs or alloy NPs with a very low (few percent) Au concentration suffer from long term surface oxidation leading to the resonance peak and scattered color shift. We have experimentally found that stability of Au/Ag alloy NPs depends on the composition [37] and long-term stability can be ensured by

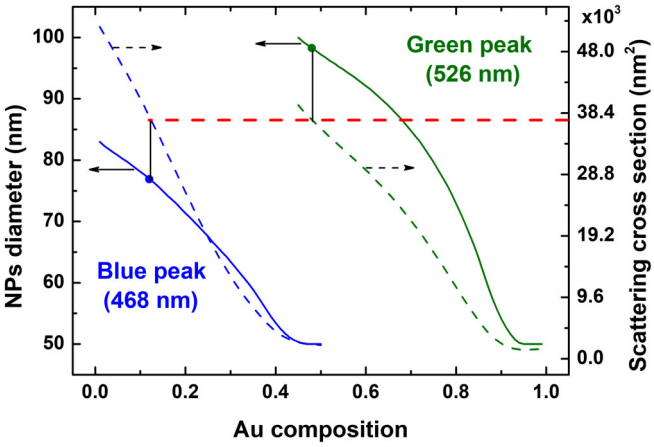

FIGURE 2 Calculation results of possible NPs diameters (solid lines) and cross sections (dashed lines) for a peak at 468 nm (blue) and at 526 nm (green) illumination in PBS. The red dashed line indicates optimization condition of a similar scattering value of 37 300 nm^2

TABLE 1 Calculated composition (in atomic percent) and size of NPs designed for RGB (peak position) illumination in three media with different RI

Medium	RI	Blue (468 nm)	Green (526 nm)	Red (638 nm)
PBS	1.34	77 nm Au/Ag 12/88[a]	99 nm Au/Ag 49/51	76-106[b] Au NR
Mounting medium	1.47	59 nm Au/Ag 10/90	80 nm Au/Ag 47/53	62-85 Au NR
Oil	1.51	52 nm Au/Ag 10/90	73 nm Au/Ag 49/51	55-75 Au NR

[a]12/88 means 12% Au and 88% Ag in composition.
[b]76-106 means nanorods of 76 nm in diameter and 106 nm in length.

at least 10% of gold in the composition. This determines the choice of "blue" NPs with 10/90 composition for mounting medium and oil, instead of theoretical 2% and 0% of gold.

The final result of the calculation and experimental optimization is presented in Table 1, including the parameters of the NPs for the other two media calculated by the similar way.

A substantial spectral shift induced by the surrounding media with higher RI such as oil and mounting medium makes it impossible to have alloy NPs with a 10/90 composition at the required resonance peak and at the reference level of scattering cross section (Au 100 nm). In these cases, our choice is to use smaller NPs with lower scattering cross sections (Figure 3), but with stable 10/90 composition which can provide long term reliability of samples analysis. Therefore, the cross section of "blue" NPs for mounting medium and oil becomes respectively ~24 800 nm^2 and ~19 100 nm^2. According to that, similar scattering cross section are set for "green" and "red" NPs in the same

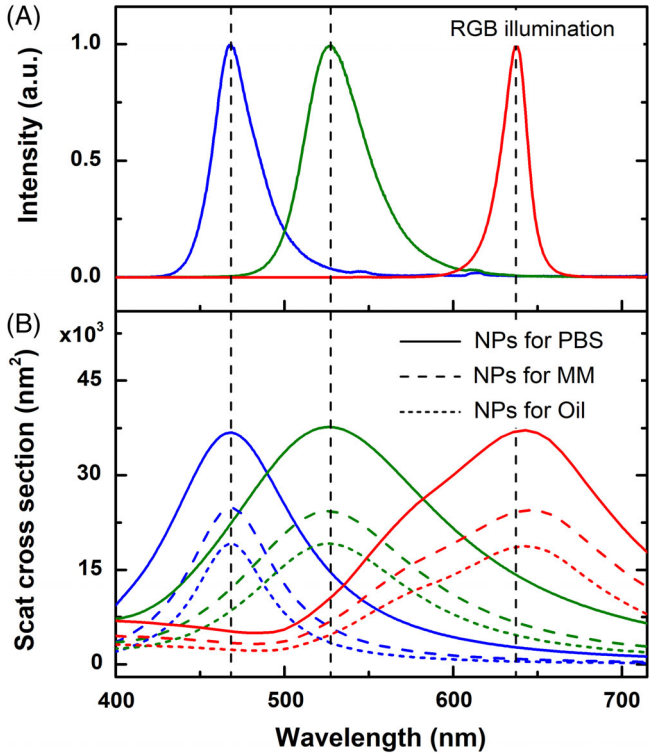

FIGURE 3 A, Spectra of normalized CL246 LED emission as RGB illumination; B, scattering cross section of designed "RGB" NPs in PBS, Vectashield mounting medium (MM) and oil, respectively. The plotting in blue, green and red represents NPs designed for corresponding color/illumination

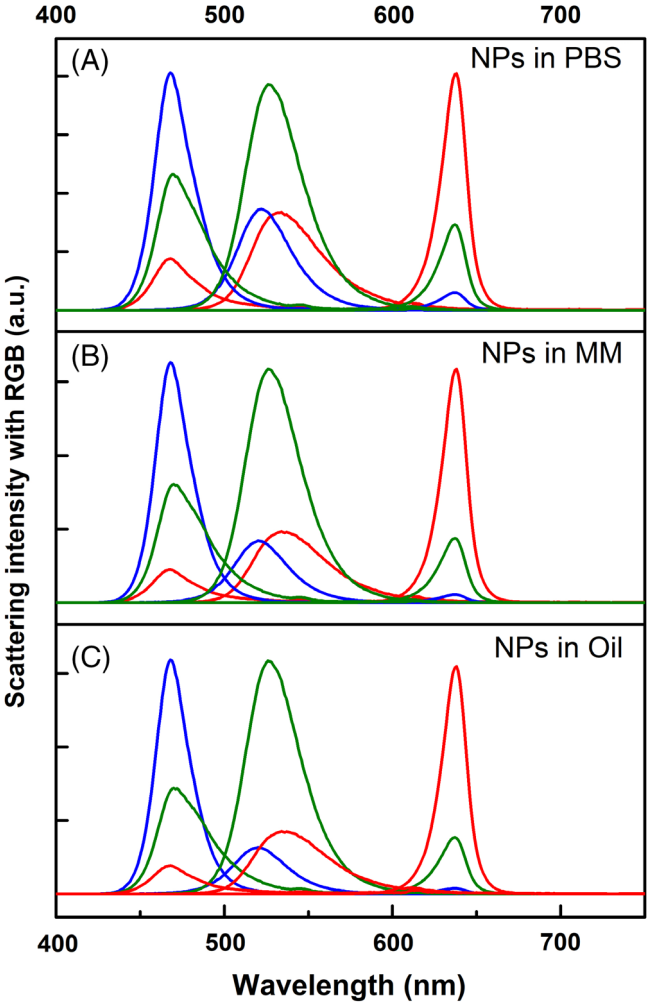

FIGURE 4 Theoretical scattering intensity of designed NPs in (A) PBS, (B) mounting medium (MM) and (C) oil, under monochromatic R, G and B illumination. The plotting in blue, green and red represents NPs designed for the corresponding color

medium. It has to be mentioned that, due to the lower light loss on the medium/glass interface, these NPs are still showing sufficiently high imaging contrast. To obtain optimal parameters of Au nanorods for work in the red spectral range and in the different media we have performed a theoretical calculation using discrete dipole scattering (nanoDDSCAT) online software [38].

Besides the scattered color under RGB illumination, visual or automatic differentiation of multiplexed plasmonic markers by the spectral signature also depends on the detected intensity contrast generated by these markers under single color illumination. Figure 4 presents the theoretical comparative scattering intensities of the three designed NPs for independent R G B illumination in each media. Almost two times higher scattering intensities for the NPs tuned to the LED color provide adequate contrast for visual differentiation of the intended markers [39]. However, in complex cellular environment, where additional scattering leads to a decrease of NPs contrast, multiplexing becomes much more reliable when all three nanoplasmonic markers are illuminated independently. In this case, visual evaluation of the three consecutive images is recommended. Fast automatic LED control with corresponding image treatment software that employs multispectral differentiation method for multiplexed NPs detection is also possible.

3.2 | Characterization of Au/Ag alloy NPs

Au/Ag alloy NPs were synthesized in accordance with the obtained theoretical results shown in Table 1. For nanorods, we chose commercially available Au nanorods from Nanopartz with similar scattering peaks as designed: diameter-length as 40 nm-80 nm for PBS and mounting medium and 40 nm-68 nm for oil. Spectral and dimensional parameters of fabricated NPs were verified by performing extinction spectroscopy of the colloidal solution, TEM and EDS. Moreover, push-broom hyperspectral imaging method was used to estimate the scattering properties of individual NPs in different surrounding media. Experimental results of the UV-visible spectral dependences of the fabricated alloy NPs in aqueous solution (not presented) are in good

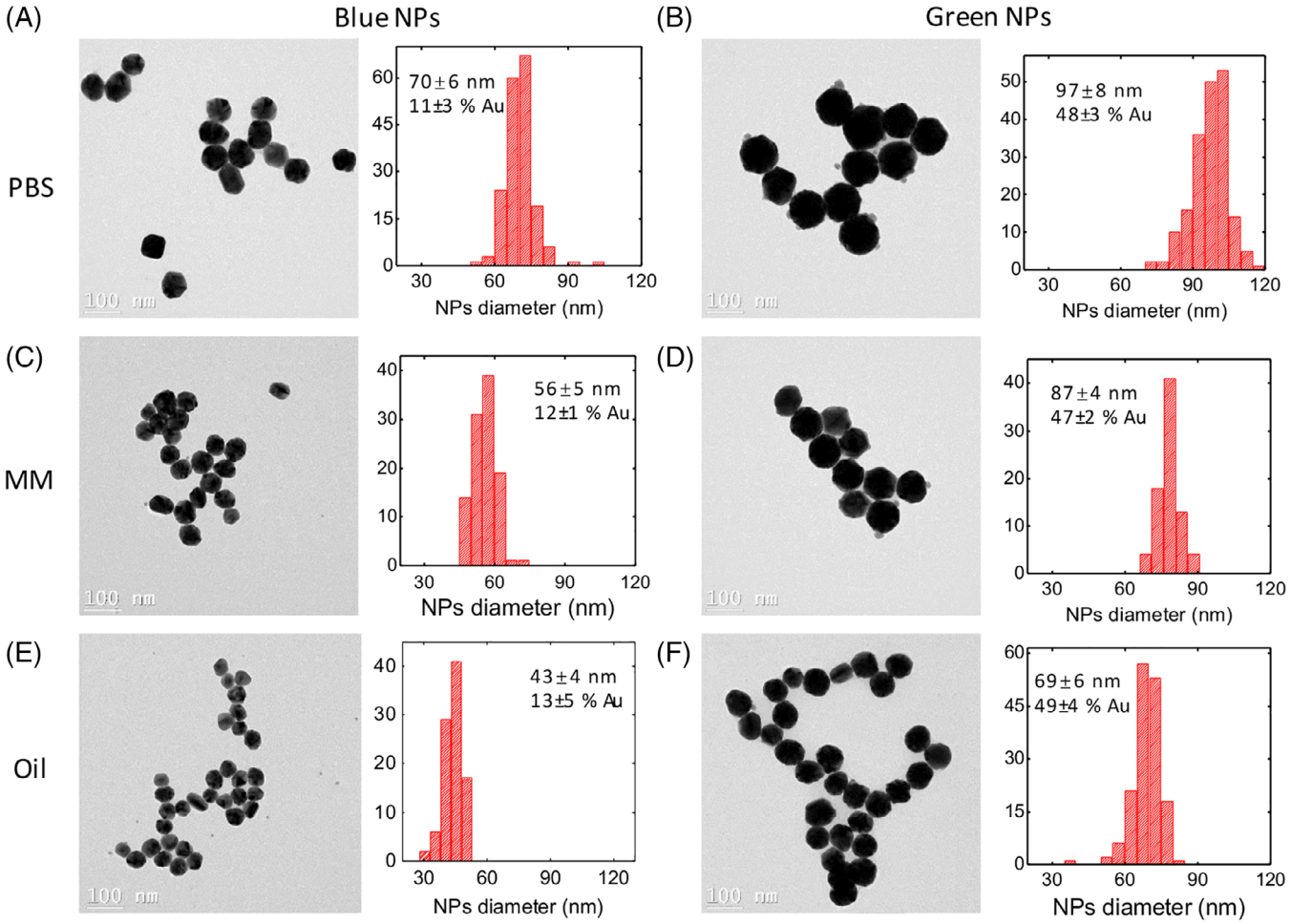

FIGURE 5 TEM images and corresponding size distribution for synthesized "blue" NPs (A, C and E) and "green" NPs (B, D and F) in PBS (A and B), mounting medium (MM) (C and D) and oil (E and F). The size (nm), the size standard deviation (nm), the gold concentration (in %) and standard deviation are given in inset for each type of NPs

agreement with the theoretical prediction from Mie theory. The experimental resonance peak position stays in less than ±15 nm deviation from the theory whereas the spectral width shows higher discrepancies. This particular parameter is directly related to the NP size distribution, which was verified by TEM. Figure 5 shows the results for the synthesized Au/Ag alloy spherical NPs designed for three working media. All mentioned characterization methods were used to estimate NPs distribution range and reproducibility of synthesis. The coefficients of variation obtained for both NP sizes and compositions remain in the acceptance 10% range, corresponding to the requirement of a reliable NPs differentiation spectral range deviation of about ±15 nm. Long-term stability of alloy NPs was verified after one-year storage in the fridge. The observed shift of the extinction spectrum was less than 5 nm for "blue" and "green" NPs that is acceptable for our optical method of spectral differentiation.

In order to spectrally characterize the NPs in experimental conditions close to real applications, we have performed push-broom hyperspectral imaging of individual NPs placed in different media between two glass slides. Conventional Halogen 50-watt microscopy illumination was used as light source, providing a smooth spectrum in the spectral range of interest. For NPs imaging, backscattering microscopy mode with 100× 1.25NA immersion oil objective was applied in order to generate high NPs contrast and 3D spatial resolution. Experimental spectral dependences presented in Figure 6 confirm that NP scattering peaks are centered or close to the corresponding LED illumination. Obtained results for the morphology, composition and finally, spectral properties of tested NPs indicate the successful synthesis of plasmonic markers for the reliable detection and spectral differentiation in the multiplexing imaging.

We have tested more than 100 NPs for each type of NPs in each medium. For each medium, under white light illumination, most spectral peaks of "blue" and "green" NPs (≥85%) are located at ±15 nm from the theoretical position. On the other hand, more than 89% of "red" NRs have a spectral peak position >600 nm, as shown in Table 2, ensuring an efficient spectral differentiation in multiplexing. For the

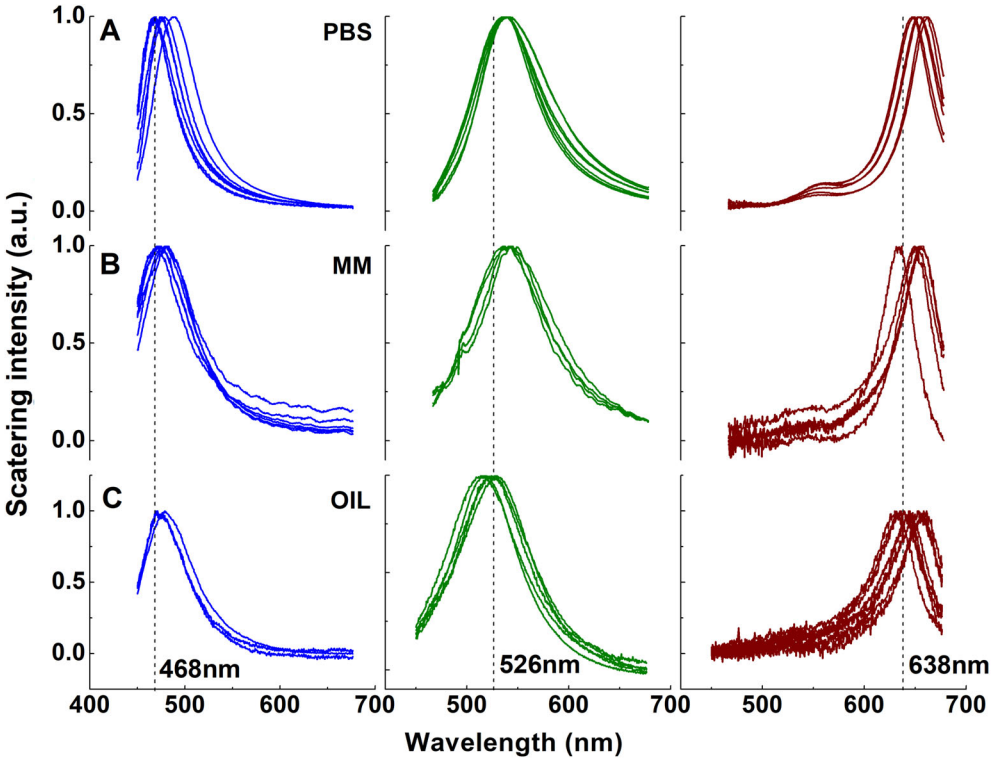

FIGURE 6 Hyperspectral examples of single NPs scattering under white (Halogen) illumination in designated medium: (A) PBS, (B) mounting medium (MM) and (C) oil, plotted in blue, green and red lines for corresponding NPs respectively. The three peak positions of RGB illumination are also indicated. For each spectrum, a sample of 5-8 nanoparticles are shown

TABLE 2 Statistical results for spectral peak (in ±15 nm range around theoretical position for "blue" and "green" NPs, >600 nm for "red" NRs) from more than 100 NPs in their targeting medium for each category

Medium	Blue NPs	Green NPs	Red NPs (> 600 nm)
PBS	87.5%	84.8%	98.0%
Mounting medium	86.7%	89.0%	92.6%
Oil	86.7%	94.0%	89.4%

nanorods chosen for the red illumination, since it is commercially available ones not exactly in optimal dimension, the spectral peak distribution is relatively wider than the ones of synthesized alloy NPs, and most of them are red-shifted compared with the red illumination. Since the red illumination is the longest wavelength and the position is quite far away from blue and green illumination, the color of nanorods stays in the red. More attention on quality control of NPs is required where influence of NPs distribution can be amplified by various parameters in practical applications.

3.3 | Multispectral plasmonic NPs imaging

Initially, multispectral plasmonic NPs imaging using dark field side illumination method with our microscopy adaptor (Figure 1) was performed in the homogeneous media. For this work, the CSI adaptor was installed on a Nikon inverted microscope stage. For each used medium (PBS, mounting medium, oil) 1 × 1 × 1 mixture of corresponding "RGB" NPs (Table 1) was placed on a 25 mm diameter glass substrate with polished side and covered by a thin glass coverslip through a 120 µm spacer. Objective 60× 0.70NA was used for the NPs visualization and Nikon color camera for the imaging.

In Figure 7A, D and G, it is possible to see NPs of three colors under the illumination of three RGB LEDs from the adaptor. In this case, NPs chromatic differentiation can be performed by the operator visual observation or by the microscope color camera. Usually "blue" and "red" NPs are readily separated, whereas differentiation of "green" NPs may sometimes be more difficult. To solve this problem, multispectral RGB imaging can be performed manually or automatically with our device. A differentiation is shown in the Figure 7. Under blue illumination, all "red" NPs disappear and on the contrary, under red light one cannot observe "blue" NPs. However, the "green" NPs while decreasing in scattered intensity are still present on the images and can be reliably identified by excluding imaging method.

3.4 | Multiplex imaging of cell samples

To demonstrate the ability of our approach and tool to provide a reliable detection method for multiplexed plasmonic NPs markers in complex cellular environment, we have performed a series of experiments with MDA-MB-231 cells cytology samples. This large and adherent breast cancer cell

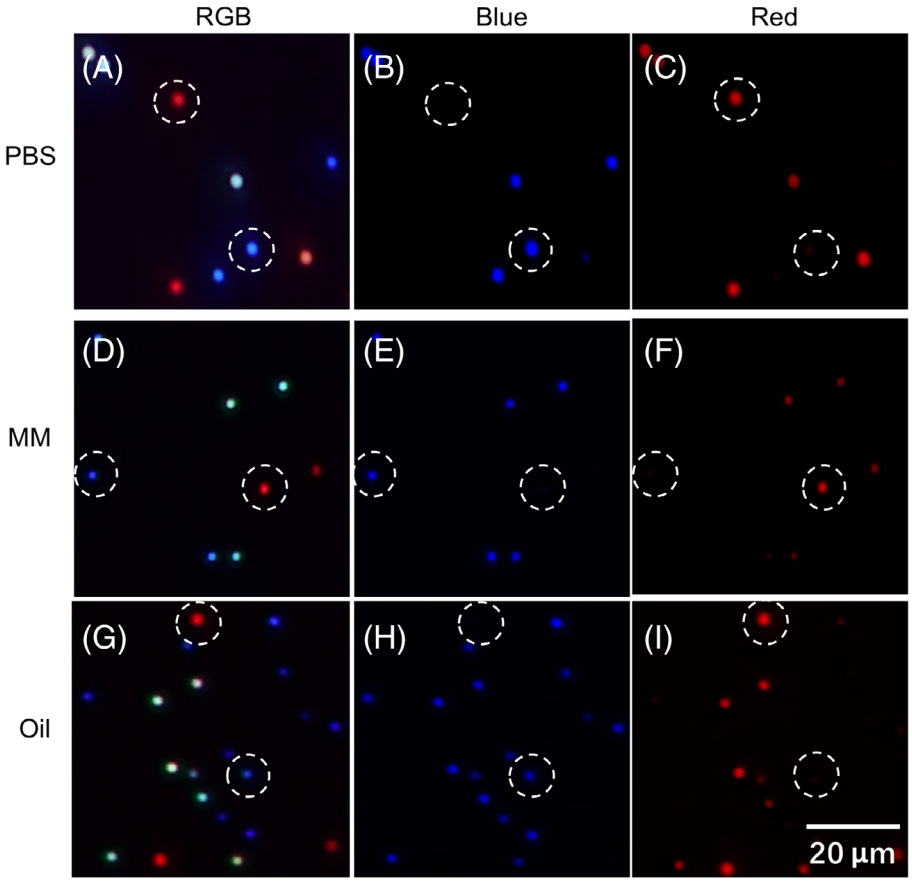

FIGURE 7 Microscopy images of NPs mixture on a glass substrate in designated medium PBS (A-C), mounting medium (MM) (D-F) and oil (G-I) under side illumination of RGB (A, D and G), single blue (B, E and F) and single red (C, F and I). The dashed circles indicate examples of one "red" NP and one "blue" NP in each medium under different illumination

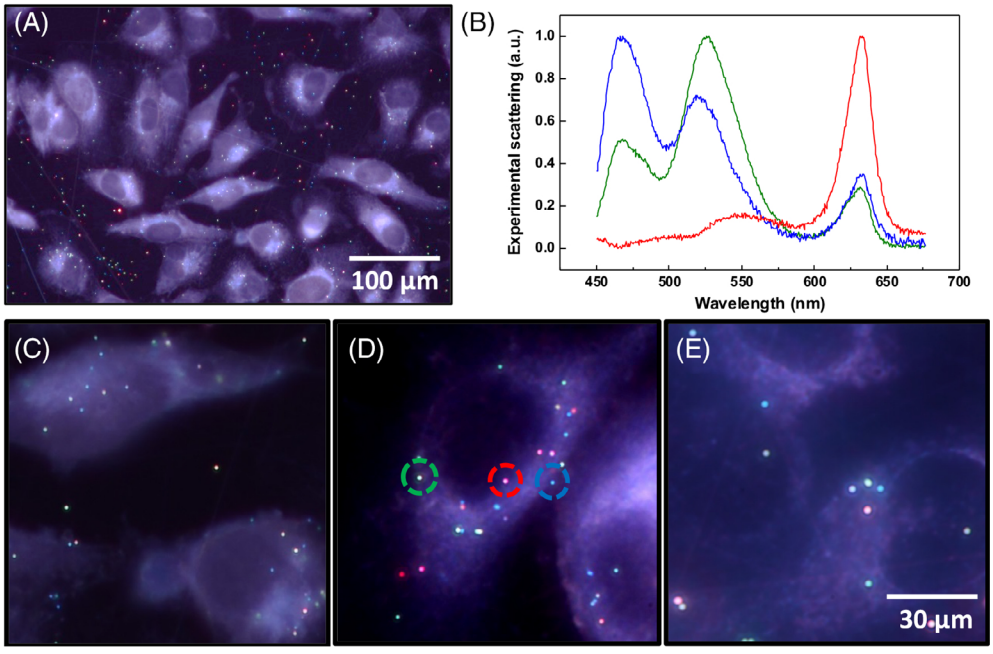

FIGURE 8 A, CSI microscopy images of NPs mixture attached on MDA-MB-231 cells; B, hyperspectrum of NPs for each color indicated in D; and detail images of NPs with cells in designated medium: C, PBS; D, mounting medium and E, oil

line is highly aggressive and poorly differentiated and there exist many studies on this cell line, since it is triple negative and difficult to have effective therapeutic methods [40, 41].

The cells were first cultured for 24 hours on the glass substrate and then mixed with the three types of NPs. After incubation, they were placed in the three different media for visualization. Figure 8 presents the typical microscopy image of MDA-MB-231 cells decorated with the different NPs mentioned above using side illumination adaptor and 60× 0.70NA objective. Corresponding color images with

higher magnification obtained in PBS, mounting medium and oil are shown in Figure 8C-E correspondingly. We can conclude from these results that direct detection and chromatic differentiation of multiple NPs in cellular environment is experimentally possible. Also, it is worth mentioning that direct microscopy visualization by human eye represents an even higher contrast in intensity and color difference than what can be shown in these figures. To further characterize plasmonic markers we have also performed a hyperspectral scan of the cells-NPs complex. With similar level of RGB illumination, the three typical spectral characteristics of NPs are shown in Figure 8B, from the ones in Figure 8D with corresponding colored circles. The spectra from each single NP are in good agreement with the one predicted by the theory (Figure 3). CSI provides also enhanced 3D spatial resolution for NPs detection compared to conventional transmission darkfield microscopy, as the proposed system has no intrinsic limitation on the maximum of the numerical aperture (NA) of the imaging objective. A z-scan has been taken for NPs-decorated cell with 60× 0.95NA objective, shown in Supplementary information.

Depending on sensitivity of human eye on different wavelengths (CIE) [42], there is still space for optimization by playing with the combination of R, G and B illumination to obtain the "white light," under which humans are used to perceive the "real color." With the development of high-power LED of various colors, the CSI approach can be even extended to other types of biomarkers of different colors, enabling an easier way of multiplexed imaging.

The demonstrated technique offers the possibility to be easily integrated in conventional diagnostics approaches used by pathologists in clinics, as well as to provide possibility for image digitization and deep learning analysis. Indeed, CSI approach balances the need of direct microscopy visualization as most widely used for practical clinic diagnosis, and the advanced digital analysis with an economic and effective way of imaging. Adaptability in current equipment and method for clinical pathologists makes our technique convenient for distribution, thus facilitating diagnosis, with fast and reliable results.

4 | CONCLUSION

Thanks to their great morphological and composition tunability, gold and gold-silver alloy nanoplasmonic biomarkers represent the potential solution for the reliable biolabeling of the cytopathology samples and efficient still simple optical detection method easily integrated on the existing microscopy setup. The synthesis method of NPs can be tailored for different scenarios depending on the final application, ensuring imaging quality and prompt direct visual analysis. The functionalization of NPs will be the next step for further use in the clinic, and will also limit non-specific attachment and aggregation [43]. Plasmonic NPs can be functionalized with various ligands, including peptides and antibodies as the most common ones for specific targeting [43, 44]. The rapidly evolving LED technology provides even more efficient and spectrally distinguishable light sources that will facilitate NPs biomarkers multiplexing with optimal image contrast. Our technology will accelerate plasmonic NPs adaptation as novel reliable and stable biological multiplexed chromatic markers for medical diagnostics.

ACKNOWLEDGMENTS

This work was supported by the financial contributions of the Fonds de Recherche du Québec Nature et Technolgie (FRQNT), the Natural Science and Engineering Research Council of Canada (NSERC) and the Canadian Institutes of Health Research (CIHR) grants. Professor Dominique Trudel receives salary support from the Fonds de Recherche du Québec-Santé (FRQS) (Clinical Research Scholar, Junior 1). Technical assistant from Yves Drolet is also acknowledged.

ORCID

Lu Wang https://orcid.org/0000-0001-9260-4933
Cecile Darviot https://orcid.org/0000-0003-4052-3079
Jennyfer Zapata-Farfan https://orcid.org/0000-0001-6270-655X
Sergiy Patskovsky https://orcid.org/0000-0001-7175-481X
Michel Meunier https://orcid.org/0000-0002-2398-5602

REFERENCES

[1] U. Aslam, S. Chavez, S. Linic, *Nat. Nanotechnol.* **2017**, *12*, 1000.
[2] H. Tong, S. X. Ouyang, Y. P. Bi, N. Umezawa, M. Oshikiri, J. H. Ye, *Adv. Mater.* **2012**, *24*, 229.
[3] Q. Z. Zhang, X. Jin, Z. H. Xu, J. M. Zhang, U. F. Rendon, L. Razzari, M. Chaker, D. L. Ma, *J. Phys. Chem. Lett.* **2018**, *9*, 5317.
[4] H. Ditlbacher, J. R. Krenn, B. Lamprecht, A. Leitner, F. R. Aussenegg, *Opt. Lett.* **2000**, *25*, 563.
[5] M. Hu, J. Chen, Z.-Y. Li, L. Au, G. V. Hartland, X. Li, M. Marquez, Y. Xia, *Chem. Soc. Rev.* **2006**, *35*, 1084.
[6] H. W. Liao, C. L. Nehl, J. H. Hafner, *Nanomedicine* **2006**, *1*, 201.
[7] N. J. Halas, S. Lal, W.-S. Chang, S. Link, P. Nordlander, *Chem. Rev.* **2011**, *111*, 3913.
[8] N. G. Khlebtsov, L. A. Dykman, *J. Quant. Spectrosc. Radiat. Transf.* **2010**, *111*, 1.
[9] W. Q. Zhu, K. B. Crozier, *Nat. Commun.* **2014**, *5*, 1.
[10] X. Huang, W. Qian, I. H. El-Sayed, M. A. El-Sayed, *Lasers Surg. Med.* **2007**, *39*, 747.
[11] R. C. Jin, *Nanoscale* **2015**, *7*, 1549.
[12] X. Sun, L. Huang, R. Zhang, W. Xu, J. Huang, D. D. Gurav, V. Vedarethinam, R. Chen, J. Lou, Q. Wang, J. Wan, K. Qian, *ACS Cent. Sci.* **2018**, *4*, 223.

[13] X. H. Huang, S. Neretina, M. A. El-Sayed, *Adv. Mater.* **2009**, *21*, 4880.
[14] A. J. Mieszawska, W. J. M. Mulder, Z. A. Fayad, D. P. Cormode, *Mol. Pharm.* **2013**, *10*, 831.
[15] L. Huang, J. Wan, X. Wei, Y. Liu, J. Huang, X. Sun, R. Zhang, D. D. Gurav, V. Vedarethinam, Y. Li, R. Chen, K. Qian, *Nat. Commun.* **2017**, *8*, 220.
[16] P. K. Jain, K. S. Lee, I. H. El-Sayed, M. A. El-Sayed, *J. Phys. Chem. B* **2006**, *110*, 7238.
[17] B. Sepulveda, P. C. Angelome, L. M. Lechuga, L. M. Liz-Marzan, *Nano Today* **2009**, *4*, 244.
[18] S. Tu, D. Rioux, J. Perreault, D. Brouard, M. Meunier, *J. Phys. Chem. C* **2017**, *121*, 8944.
[19] Y. Park, C. Depeursinge, G. Popescu, *Nat. Photon.* **2018**, *12*, 578.
[20] J. A. Webb, R. Bardhan, *Nanoscale* **2014**, *6*, 2502.
[21] W. Chen, S. Zhang, Y. Yu, H. Zhang, Q. He, *Adv. Mater.* **2016**, *28*, 8567.
[22] M. Qi, C. Darviot, S. Patskovsky, M. Meunier, *Analyst* **2019**, *144*, 1303.
[23] A. Madabhushi, G. Lee, *Med. Image Anal.* **2016**, *33*, 170.
[24] D. Rioux, M. Meunier, *J. Phys. Chem. C* **2015**, *119*, 13160.
[25] J. Turkevich, P. C. Stevenson, J. Hillier, *Discuss. Faraday Soc.* **1951**, *11*, 55.
[26] X. Dong, X. Ji, H. Wu, L. Zhao, J. Li, W. Yang, *J. Phys. Chem. C* **2009**, *113*, 6573.
[27] N. G. Bastús, F. Merkoçi, J. Piella, V. Puntes, *Chem. Mater.* **2014**, *26*, 2836.
[28] R. Baber, L. Mazzei, N. T. K. Thanh, A. Gavriilidis, *Nanoscale* **2017**, *9*, 14149.
[29] S. Patskovsky, E. Bergeron, D. Rioux, M. Simard, M. Meunier, *Analyst* **2014**, *139*, 5247.
[30] G. Doria, J. Conde, B. Veigas, L. Giestas, C. Almeida, M. Assuncao, J. Rosa, P. V. Baptista, *Sensors* **2012**, *12*, 1657.
[31] T. L. Doane, C. Burda, *Chem. Soc. Rev.* **2012**, *41*, 2885.
[32] S. Patskovsky, E. Bergeron, M. Meunier, *J. Biophoton.* **2015**, *8*, 162.
[33] S. Zhang, J. Li, G. Lykotrafitis, G. Bao, S. Suresh, *Adv. Mater.* **2009**, *21*, 419.
[34] R. Garcia-Alvarez, M. Hadjidemetriou, A. Sanchez-Iglesias, L. M. Liz-Marzan, K. Kostarelos, *Nanoscale* **2018**, *10*, 1256.
[35] G. Mie, *Ann. Phys.* **1908**, *330*, 377.
[36] D. Rioux, S. Vallières, S. Besner, P. Muñoz, E. Mazur, M. Meunier, *Adv. Opt. Mater.* **2014**, *2*, 176.
[37] C. Gao, Y. Hu, M. Wang, M. Chi, Y. Yin, *J. Am. Chem. Soc.* **2014**, *136*, 7474.
[38] P. K. Jain, N. Sobh, J. Smith, A. N. Sobh, S. White, J. Faucheaux, J. Feser in nanoDDSCAT, https://nanohub.org/resources/dda (accessed: March 2019).
[39] A. Rose, *J. Opt. Soc. Am.* **1948**, *38*, 196.
[40] H. S. Jung, J. Han, H. Shi, S. Koo, H. Singh, H.-J. Kim, J. L. Sessler, J. Y. Lee, J.-H. Kim, J. S. Kim, *J. Am. Chem. Soc.* **2017**, *139*, 7595.
[41] M. Milczarek, K. Wiktorska, L. Mielczarek, M. Koronkiewicz, A. Dąbrowska, K. Lubelska, D. Matosiuk, Z. Chilmonczyk, *Food Chem. Toxicol.* **2018**, *111*, 1.
[42] T. Smith, J. Guild, *Trans. Opt. Soc.* **1931**, *33*, 73.
[43] E. Bergeron, C. Boutopoulos, R. Martel, A. Torres, C. Rodriguez, J. Niskanen, J.-J. Lebrun, F. M. Winnik, P. Sapieha, M. Meunier, *Nanoscale* **2015**, *7*, 17836.
[44] S. Monti, G. Barcaro, L. Sementa, V. Carravetta, H. Ågren, *Nano Res.* **2018**, *11*, 1757.

SUPPORTING INFORMATION

Additional supporting information may be found online in the Supporting Information section at the end of this article.

How to cite this article: Wang L, Darviot C, Zapata-Farfan J, Patskovsky S, Trudel D, Meunier M. Designable nanoplasmonic biomarkers for direct microscopy cytopathology diagnostics. *J. Biophotonics*. 2019;12:e201900166. https://doi.org/10.1002/jbio.201900166